PAPER Special Section on Analog Circuit Techniques and Related Topics

A Reduction Technique for RLCG Interconnects Using Least Squares Method

Junji KAWATA[†a)], **Yuichi TANJI**[††], **Yoshifumi NISHIO**[†††], ***Members***, ***and*** **Akio USHIDA**[†], ***Fellow***

SUMMARY In this paper, we propose a new algorithm for calculating the exact poles of the admittance matrix of RLCG interconnects. After choosing dominant poles and corresponding residues, each element of the exact admittance matrix is approximated by partial fraction. A procedure to obtain the residues that guarantee the passivity is also provided, based on experimental studies. In the procedure the residues are calculated by using the least squares method so that the partial fraction matches each element of the exact admittance matrix in the frequency-domain. From the partial fraction representation, the asymptotic equivalent circuit models which can be easily simulated with SPICE are synthesized. It is shown that an efficient model-order reduction is possible for short-length interconnects.

key words: *RLCG interconnects, Leverrier-Faddeeva algorithm, least squares method, passivity, asymptotic equivalent circuits, reduction*

1. Introduction

The analysis and design of high speed LSI chips are becoming more and more important, because the sub-circuits coupled with interconnects embedded in the substrate sometimes cause the fault switching operations due to the signal delays, crosstalks, reflections and so on [1]–[5]. The Elmore resistance-capacitance (RC) delay metric is popular due to its simple closed-form expression, computation speed and fidelity with respect to the simulation [4]. The closed-form combining with the delay and crosstalk is firstly presented in the reference [5]. The modified algorithms are proposed later for the improvement of the accuracy and the practical applications in the simulations [6]–[9].

AWE (asymptotic waveform evaluation method) [10] is widely used as a reduction technique of the large scale of linear networks, the algorithm is based on a moment-matching technique and Padé approximation. However, the method sometimes become erroneous, if there exist the poles far from the origin. To overcome the problem, CFH (complex frequency hopping) [11] and multi-point Padé approximation [12] methods are proposed. In these reduction algorithms, the reduced circuits sometimes become unstable in the time domain even if all the poles are located in the left hand side of the complex plane. The ill-condition can be overcome by PVL (Padé via Lanczos process) [13], and PRIMA (passive reduced-order interconnect macromodeling algorithm) [2], [14]. In order to apply these algorithms to the interconnects, we need two steps such that each interconnect is firstly modeled by a finite order system, and Arnoldi-based congruence transformation is applied to the system to form its reduced order model.

In this paper, we consider LSIs such as ASIC or SoC (System on a Chip) are coupled with interconnects embedded in the substrate. In this case, the diffusion resistance components of the interconnects are generally assumed to be very large compared to those of PCBs [3] and the lengths are very short. From the telegrapher's equation of the interconnects, the admittance matrix can be derived from the relations at the near and far ends [1]. We propose here a new computational algorithm for calculating the *exact poles* in the complex plane. Next, each of the elements of the admittance matrix is approximated by partial fraction using dominant poles around the origin, where the corresponding residues are evaluated by the least squares method. A computational procedure to obtain the residues that guarantee the passivity is also provided. Thus, the admittance matrix are reduced as the partial fractions and are subsequently synthesized as asymptotic equivalent circuits.

We present the numerical methods for calculating the exact poles and corresponding residues in Sect. 2. Section 2.3 shows the asymptotic equivalent circuits of the interconnects. Illustrative examples are given in Sect. 3. First, distribution of poles for some cases is investigated. Then, using the residues estimated by the least squares method, we calculate the frequency response curves and compared them with the exact ones. Here, it will be investigated that how the passivity of partial fractions obtained from pole-residue pairs breaks and why inaccurate residues are obtained. Based on the considerations, we provide a procedure to guarantee the passivity of the asymptotic circuits. Furthermore, SPICE simulations using the asymptotic equivalent circuit and the built-in lossy transmission line model of SPICE are carried out and the transient waveforms are compared. It is found that the transient responses obtained by the macromodels are in good agreement with those of SPICE model as the number of poles increases, and that the order of partial fractions can be efficiently reduced for short-length interconnects.

Manuscript received June 20, 2004.
Manuscript revised September 15, 2004.
Final manuscript received October 20, 2004.

[†]The authors are with the Faculty of Engineering, Tokushima Bunri University, Sanuki-shi, 769-2193 Japan.
[††]The author is with the Faculty of Engineering, Kagawa University, Takamatsu-shi, 761-0396 Japan.
[†††]The author is with the Faculty of Engineering, Tokushima University, Tokushima-shi, 770-8506 Japan.
a) E-mail: kawata@fe.bunri-u.ac.jp

2. Calculation of Exact Poles of Interconnects

2.1 Admittance Matrix of Interconnects and Its Poles

Now, consider a uniform N coupled RLCG interconnects described by the following telegrapher's equations:

$$\left.\begin{aligned}\frac{d\mathbf{V}(x,s)}{dx} &= -(\mathbf{R}+s\mathbf{L})\mathbf{I}(x,s)\\ \frac{d\mathbf{I}(x,s)}{dx} &= -(\mathbf{G}+s\mathbf{C})\mathbf{V}(x,s)\end{aligned}\right\} \tag{1}$$

where, $\mathbf{V}(x,s) \in \mathcal{R}^N$ and $\mathbf{I}(x,s) \in \mathcal{R}^N$ are the voltage and current vectors at x, and $\mathbf{R} \in \mathcal{R}^{N\times N}$, $\mathbf{L} \in \mathcal{R}^{N\times N}$,$\mathbf{C} \in \mathcal{R}^{N\times N}$ and $\mathbf{G} \in \mathcal{R}^{N\times N}$ are the resistance, inductance, capacitance and conductance matrices per unit length, respectively. These are non-negative definite symmetric matrices. From (1), we have

$$\left.\begin{aligned}\frac{d\mathbf{V}^2(x,s)}{dx} &= (\mathbf{R}+s\mathbf{L})(\mathbf{G}+s\mathbf{C})\mathbf{V}(x,s)\\ \frac{d\mathbf{I}^2(x,s)}{dx} &= (\mathbf{G}+s\mathbf{C})(\mathbf{R}+s\mathbf{L})\mathbf{I}(x,s)\end{aligned}\right\} \tag{2}$$

Let us introduce the transform matrices $\mathbf{P}_v(s)$ and $\mathbf{P}_c(s)$ in order to transform (2) into diagonal forms. Thus, we have

$$\left.\begin{aligned}\mathrm{diag}[\gamma_i(s)^2] &= \mathbf{P}_v(s)^{-1}(\mathbf{R}+s\mathbf{L})(\mathbf{G}+s\mathbf{C})\mathbf{P}_v(s)\\ \mathrm{diag}[\gamma_i(s)^2] &= \mathbf{P}_c(s)^{-1}(\mathbf{G}+s\mathbf{C})(\mathbf{R}+s\mathbf{L})\mathbf{P}_c(s)\end{aligned}\right\} \tag{3}$$

When a complex frequency s is given, the eigenvalues $\gamma_i(s)^2$ and the corresponding eigenvectors can be uniquely obtained. Because $\mathbf{P}_v(s)$ and $\mathbf{P}_c(s)$ have the eigenvectors as the columns, these matrices can be also uniquely determined for the complex frequency s. $\mathbf{P}_c(s)$ satisfies the following relations:

$$\mathbf{P}_c(s) = (\mathbf{R}+s\mathbf{L})^{-1}\mathbf{P}_v(s)\mathbf{\Gamma}(s) \tag{4}$$

$$\mathbf{P}_c^T(s) = \mathbf{P}_v(s)^{-1} \tag{5}$$

for $\mathbf{\Gamma}(s) = \mathrm{diag}[\gamma_i(s)]$. Then, the input and output relations at the near and far ends are described by the admittance matrix as follows [1]:

$$\begin{bmatrix}\mathbf{I}(0,s)\\ \mathbf{I}(d,s)\end{bmatrix} = \begin{bmatrix}\mathbf{Y}_{11}(s) & \mathbf{Y}_{12}(s)\\ \mathbf{Y}_{21}(s) & \mathbf{Y}_{22}(s)\end{bmatrix}\begin{bmatrix}\mathbf{V}(0,s)\\ \mathbf{V}(d,s)\end{bmatrix} \tag{6}$$

where d is the length of the interconnects, and $\{\mathbf{V}(0,s), \mathbf{V}(d,s)\}$ and $\{\mathbf{I}(0,s), \mathbf{I}(d,s)\}$ denote the terminal voltage and current vectors of the interconnects, respectively. The submatrices $\mathbf{Y}_{ij}(s) \in \mathcal{R}^{N\times N}$ of the admittance matrix are given by:

$$\left.\begin{aligned}&\mathbf{Y}_{11}(s) = \mathbf{Y}_{22}(s)\\ &\quad = \mathbf{P}_c(s)\mathrm{diag}[\coth\gamma_i(s)d]\mathbf{P}_v(s)^{-1}\\ &\mathbf{Y}_{12}(s) = \mathbf{Y}_{21}(s)\\ &\quad = -\mathbf{P}_c(s)\mathrm{diag}\left[\frac{1}{\sinh\gamma_i(s)d}\right]\mathbf{P}_v(s)^{-1}\end{aligned}\right\} \tag{7}$$

Observe that all the poles of admittance matrix can be found at the locations satisfying $\sinh\gamma_i(s) = 0,\ \ i = 1,2,\ldots,N$. Thus, we have the following theorem for calculation of the exact poles.

Theorem 1: The locations of poles satisfying the relations (7) are found by solving the following equation:

$$\left|(\mathbf{R}+s\mathbf{L})(\mathbf{G}+s\mathbf{C}) + \left(\frac{n\pi}{d}\right)^2\mathbf{I}\right| = 0,\ \ n = 1,2,\ldots \tag{8}$$

Proof: In the case of $n \neq 0$, we have from (7) that the poles satisfy the following relations:

$$|\mathbf{P}_v(s)\mathrm{diag}[\sinh\gamma_i(s)d]\mathbf{P}_c(s)^{-1}| = 0 \tag{9}$$

$$|\mathbf{P}_v(s)\mathrm{diag}[\tanh\gamma_i(s)d]\mathbf{P}_c(s)^{-1}| = 0 \tag{10}$$

Since the transform matrices $\mathbf{P}_v(s)$ and $\mathbf{P}_c(s)$ are nonsingular for the nonzero eigenvalues, the poles satisfying the above two relations are given by

$$\gamma_i(s)d = jn\pi,\quad i = 1,2,\ldots,N,\ \ n = 1,2,\ldots$$

Therefore, the characteristic equation from the telegrapher's equation (1) has to satisfy the relation (8). Q.E.D.

Corollary 1.1: The poles at $n = 0$ satisfy the following relation:

$$|\mathbf{R}+s\mathbf{L}| = 0 \tag{11}$$

Proof: We have $\gamma_i = 0$ at $n = 0$. Thus, using the relation of (4), we have the following relation:

$$\begin{aligned}&\lim_{\gamma_i\to 0}\mathbf{P}_c(s)\mathrm{diag}\left[\frac{1}{\sinh\gamma_i(s)d}\right]\mathbf{P}_v(s)^{-1}\\ &\quad = (\mathbf{R}+s\mathbf{L})^{-1}\mathbf{P}_v(s)\mathrm{diag}[\gamma_i(s)]\frac{1}{\mathrm{diag}[\gamma_i(s)d]}\mathbf{P}_v(s)^{-1}\\ &\quad = \frac{1}{d}(\mathbf{R}+s\mathbf{L})^{-1}\end{aligned} \tag{12}$$

Q.E.D.

2.2 Numerical Methods for Calculating Exact Poles

Generally, it is not easy to calculate the poles using the relation (8). Hence, we apply Leverrier-Faddeeva algorithm [16] in order to obtain the characteristic equation $|s\mathbf{I}-\mathbf{A}| = 0$ for the relation (8). Setting (8) into

$$\mathbf{A}(s) = -(\mathbf{RC}+\mathbf{LG})^{-1}\left[\mathbf{RG}+\left(\frac{n\pi}{d}\right)^2\mathbf{I}+s^2\mathbf{LC}\right] \tag{13}$$

we have

$$|s\mathbf{I}-\mathbf{A}(s)| = \alpha_0(s)+s\alpha_1(s)+\cdots+s^{N-1}\alpha_{N-1}(s)+s^N \tag{14}$$

where $\alpha_k(s)$ is found by the following recurrence formulae:

$$\left.\begin{aligned}&\mathbf{B}_{N-1} = \mathbf{I},\\ &\quad\Rightarrow\ \ \alpha_{N-1}(s) = -\mathrm{tr}(\mathbf{A}(s))\\ &\mathbf{B}_{N-2}(s) = \mathbf{A}(s)\mathbf{B}_{N-1}+\alpha_{N-1}(s)\mathbf{I},\\ &\quad\Rightarrow\ \ \alpha_{N-2}(s) = -\frac{1}{2}\mathrm{tr}(\mathbf{B}_{N-2}(s)\mathbf{A}(s))\\ &\cdots\cdots\cdots\cdots\cdots\cdots\cdots\cdots\\ &\mathbf{B}_0(s) = \mathbf{A}(s)\mathbf{B}_1(s)+\alpha_1(s)\mathbf{I},\\ &\quad\Rightarrow\ \ \alpha_0(s) = -\frac{1}{N}\mathrm{tr}(\mathbf{B}_0(s)\mathbf{A}(s))\end{aligned}\right\} \tag{15}$$

Note that the maximum degree of (14) eventually becomes $2N$, because $\alpha_k(s)$ is polynomial with s. This algebraic equation can be numerically solved by the use of Bairstow method and so on. In this way, we can calculate the exact poles of the admittance matrix (7).

We choose dominant poles located around the origin of complex plane, because the poles have large influence on the transient responses. Thus, an arbitrary (i, j) element of the submatrices $\mathbf{Y}_{11}(s)$, $\mathbf{Y}_{12}(s)$, $\mathbf{Y}_{21}(s)$, and $\mathbf{Y}_{22}(s)$ of (7) is approximated by the partial fractions that is composed of the dominant poles and the corresponding residues, in the following forms[†]:

$$\hat{Y}_{11}(s) = \hat{Y}_{22}(s) = \sum_{i=1}^{N} \frac{k_{01,i}}{s - p_{0,i}} + \sum_{i=1}^{N} \sum_{n=1}^{M} \frac{b_{11,i,n}s + b_{10,i,n}}{s^2 + a_{1,i,n}s + a_{0,i,n}} \tag{16}$$

$$\hat{Y}_{12}(s) = \hat{Y}_{21}(s) = \sum_{i=1}^{N} \frac{k_{02,i}}{s - p_{0,i}} + \sum_{i=1}^{N} \sum_{n=1}^{M} \frac{b_{21,i,n}s + b_{20,i,n}}{s^2 + a_{1,i,n}s + a_{0,i,n}} \tag{17}$$

where N is the number of conductors and M shows the number of complex conjugate pairs for each $\gamma_i(s)$.

It has been shown in [18] that the absolute values of residues are the same, but their signs change alternately with n; i.e.,

$$\left.\begin{aligned} k_{02,i} &= -k_{01,i} \\ b_{21,i,n} &= (-1)^{n+1} b_{11,i,n} \\ b_{20,i,n} &= (-1)^{n+1} b_{10,i,n} \end{aligned}\right\} \tag{18}$$

Therefore, there is no need to evaluate the residues for (17). Equations (16) and (17) are divided into two parts depending on whether n is odd or even, where the first term in the equations corresponds to the case of $n = 0$ and is included in the even part. Since all elements of the approximated submatrices $\hat{\mathbf{Y}}_{11}$, $\hat{\mathbf{Y}}_{12}$, $\hat{\mathbf{Y}}_{21}$, and $\hat{\mathbf{Y}}_{22}$ are separated into the odd and even parts, we can express the submatrices with the two new submatrices $\mathbf{Y}_a$ and $\mathbf{Y}_b$ as follows.

$$\begin{bmatrix} \hat{\mathbf{Y}}_{11}(s) & \hat{\mathbf{Y}}_{12}(s) \\ \hat{\mathbf{Y}}_{21}(s) & \hat{\mathbf{Y}}_{22}(s) \end{bmatrix} = \begin{bmatrix} \mathbf{Y}_a(s)+\mathbf{Y}_b(s) & \mathbf{Y}_a(s)-\mathbf{Y}_b(s) \\ \mathbf{Y}_a(s)-\mathbf{Y}_b(s) & \mathbf{Y}_a(s)+\mathbf{Y}_b(s) \end{bmatrix} \tag{19}$$

where $\mathbf{Y}_a$ and $\mathbf{Y}_b$ are corresponding to the odd and even parts, respectively. The asymptotic equivalent circuit models to be synthesized must satisfy the relations (16)–(19).

2.3 Asymptotic Equivalent Circuit of Interconnects

In this subsection, we derive the asymptotic equivalent circuit models that satisfy the relations (16)–(19). Each term of partial fractions (16) and (17) is synthesized by the circuit models shown in Figs. 1(a) and (b), where the circuit parameters are given by

$$L_{i,0} = \frac{1}{k_{0,i}}, \quad R_{i,0} = \frac{p_{0,i}}{k_{0,i}} \tag{20}$$

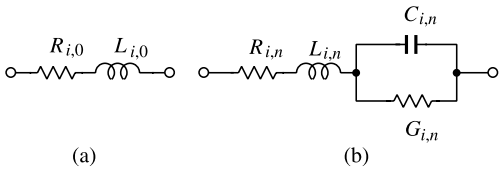

Fig. 1 Equivalent circuit models of each term in the partial fractions (16) and (17).

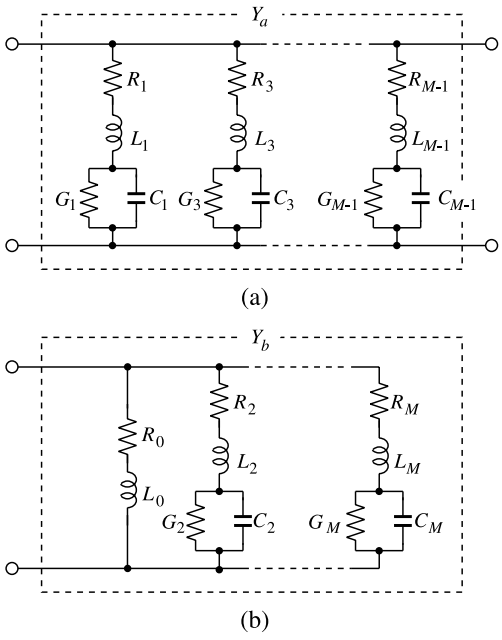

Fig. 2 Equivalent circuit models of the matrix (19) for single-conductor interconnect. (a) Y_a and (b) Y_b.

$$\left.\begin{aligned} L_{i,n} &= \frac{1}{b_{1,i,n}}, \quad R_{i,n} = \frac{a_{1,i,n}b_{1,i,n} - b_{0,i,n}}{b_{1,i,n}^2} \\ C_{i,n} &= \frac{b_{1,i,n}^3}{a_{0,i,n}b_{1,i,n}^2 + (b_{0,i,n} - a_{1,i,n}b_{1,i,n})b_{0,i,n}} \\ G_{i,n} &= \frac{b_{1,i,n}^2 b_{0,i,n}}{a_{0,i,n}b_{1,i,n}^2 + (b_{0,i,n} - a_{1,i,n}b_{1,i,n})b_{0,i,n}} \end{aligned}\right\} \tag{21}$$

Each element of the admittance matrix (19) is modeled by parallel connection of the sub-circuits shown in Fig. 1. For example, in the case of single-conductor interconnect, we have the circuits shown in Fig. 2 for $\mathbf{Y}_a(s)$ and $\mathbf{Y}_b(s)$, where the subscript i is omitted for simplicity. In the case of single-conductor interconnect, we can construct two equivalent circuit models in the different forms shown in Figs. 3 and 4(a), where $I_r(0, s)$ and $I_r(d, s)$ in Fig. 4(a) are the voltage-controlled current sources given by Figs. 4(b) and 4(c). Observe that the circuit of Fig. 3 does not contain any controlled source, so that the circuit is passive if all of the circuit parameters have positive values. Also, it should be noted that the circuit shown in Fig. 4(a) is passive if the circuit shown in Fig. 3 is passive. The macromodels can

[†]To avoid confusion about suffix notation, the suffix (i, j) is omitted in (16)–(17).

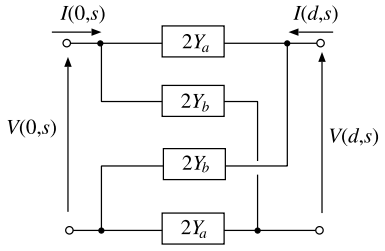

Fig. 3 Equivalent circuit model for single-conductor interconnect using a bridge circuit.

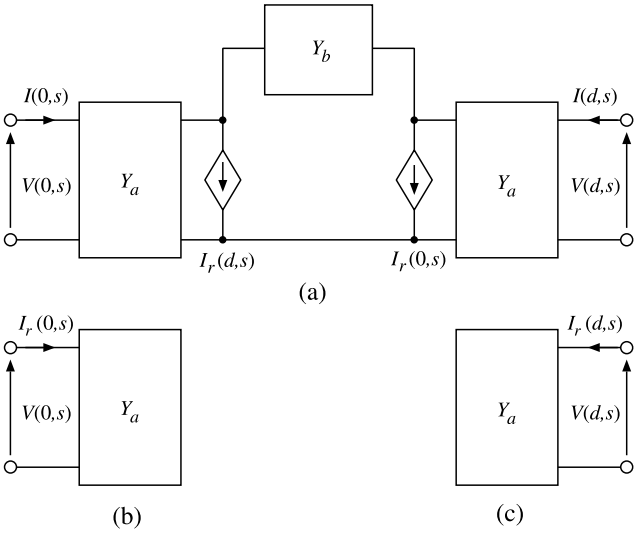

Fig. 4 Equivalent circuit models for single-conductor interconnect. The subsystems Y_a and Y_b are shown in Fig. 2.

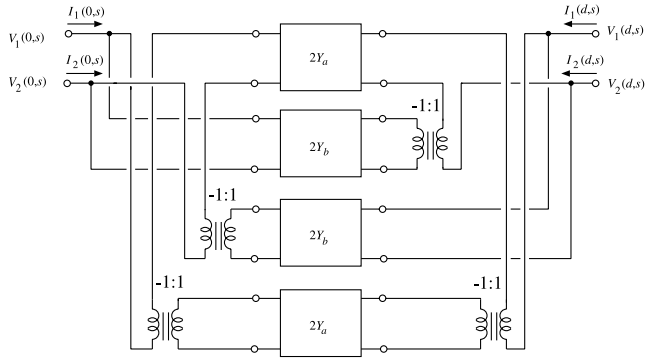

Fig. 5 Equivalent circuit model to two-conductors interconnect.

be easily implemented on any kind of SPICE-like simulators, since the asymptotic circuits are composed of typical circuit elements only. The model of two conductors interconnect is realized by the use of 4 current transformers as shown in Fig. 5. The asymptotic equivalent circuit for multi-conductor interconnect is shown in Fig. 6, which is easily modeled with SPICE.

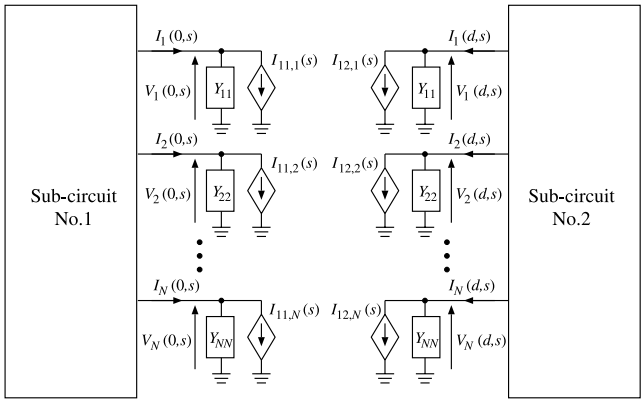

Fig. 6 Equivalent circuit model to multi-conductor interconnect.

2.4 Numerical Procedure for Calculating Residues

The residues satisfying (16) can be calculated by the least squares method. The frequency response curve of each element of the admittance matrix (7) must be matched to the exact one, namely $Y(s_k) = \hat{Y}(s_k)$ at sampled frequency points $s_k,\ k = 1, \ldots, K$. Thus we have

$$\mathbf{AX} = \mathbf{B} \tag{22}$$

where $\mathbf{X}$ is unknown vector containing the residues, and $\mathbf{B}$ is column vector consisted of exact sampled frequency-domain data:

$$\mathbf{X} = \left[\, k_{0,1} \ \cdots \ k_{0,N} \ b_{1,1,1} \ b_{0,1,1} \ \cdots \ b_{1,N,M} \ b_{0,N,M} \,\right]^T \tag{23}$$

$$\mathbf{B} = \left[\, Y(s_1) \ Y(s_2) \ \cdots \ Y(s_K) \,\right]^T \tag{24}$$

and each element of $\mathbf{A}$ is given as:

$$A_{k,j} = \frac{1}{s_k - p_{0,j}}, \quad j = 1, \ldots, N \tag{25}$$

$$\left.\begin{aligned} A_{k,N+2j-1} &= \frac{s_k}{s_k^2 + a_{1,j} s_k + a_{0,j}} \\ A_{k,N+2j} &= \frac{1}{s_k^2 + a_{1,j} s_k + a_{0,j}} \end{aligned}\right\}, \tag{26}$$

$$j = (i-1)M + n,\ i = 1, \ldots, N,\ n = 1, \ldots, M$$

The least squares solution $\mathbf{X}$ can be found by using QR factorization so that $\|\mathbf{B} - \mathbf{AX}\|_2$ is minimized.

In order to guarantee the passivity of the macromodels, the following trial-and-error approach for calculating the residues is provided. In Sect. 3, it will be explained in detail how the following procedure ensures the passivity of the macromodels.

Step 1) Determine the highest frequency f_{max} considering the frequency spectrum of input pulse signals.

Step 2) Choose all poles with the imaginary part less than or equal to $2\pi f_{max}$ and further several extra poles beyond the frequency. Let the number of the former and the latter be M and α, respectively. Thus the value of

M in (23) and (26) is replaced with $M_{ext} = M + \alpha$. The appropriate initial value of α is about $5 \sim 10$.

Step 3) Perform the least squares fitting and subsequently truncate the extra α pole-residue pairs beyond $2\pi f_{max}$.

Step 4) If all of the residues (23) and the resulting circuit parameters (20) and (21) are positive, finish the computation; otherwise increase the number of extra poles α and return to Step 3.

It should be noted that the proposed method enforces the passivity of the interconnect macromodels. All the values of the passive elements included in the macromodels are constrained to be positive. Hence, the macromodels are guaranteed to be passive.

3. Illustrative Examples

3.1 Distribution of Poles

First, we investigate distribution of poles in the complex plane by the computational method described in the subsection 2.2, because this gives us very important information to choose dominant poles. The parameters of interconnects are set as follows:

$R_{i,i} = r\,[\Omega/\mathrm{mm}]$, other elements of $\mathbf{R}$ are 0.
$L_{i,i} = 10\,[\mathrm{nH/mm}], L_{i,i+1} = L_{i-1,i} = 1\,[\mathrm{nH/mm}]$,
$L_{i,i+2} = L_{i-2,i} = 0.1\,[\mathrm{nH/mm}]$, other elements of $\mathbf{L}$ are 0.
$C_{i,i} = 4\,[\mathrm{pF/mm}], C_{i,i+1} = C_{i-1,i} = -0.21\,[\mathrm{pF/mm}]$,
$C_{i,i+2} = C_{i-2,i} = -0.01\,[\mathrm{pF/mm}]$, other elements of $\mathbf{C}$ are 0.
$G_{i,i} = 0.5\,[\mathrm{mS/mm}], G_{i,i+1} = G_{i-1,i} = -0.05\,[\mathrm{mS/mm}]$,
$G_{i,i+2} = G_{i-2,i} = -0.01\,[\mathrm{mS/mm}]$, other elements of $\mathbf{G}$ are 0.

and the values of N, r and d (resp., the number of conductors, the resistance component and the length of interconnect) are changed in the examples.

Figure 7 shows distribution of poles for interconnects with different values of N. The poles with negative imaginary part are not shown in these figures. Observe that they consist of N real poles and complex conjugate poles for each n in (8). As shown in Fig. 7 the imaginary parts of the complex conjugate poles increase monotonically as n in (8). We assume an input pulse waveform which has large spectrum in the lower frequency range. Thus model accuracy in the lower frequency range, which is closely related to poles located near the origin, is very important for transient simulations. Since poles for large n are far from the origin, they do not play important roles for the transient responses.

Next, either the length d or the resistance component r of 4-conductors interconnect is changed and the distributions are examined. The results are shown in Fig. 8. Compared Fig. 7(c) with Fig. 8(a), it is obvious that the imaginary parts of the poles for short-length interconnect become quickly large for n. Further, from Figs. 7(c) and 8(b), we found that the real parts of poles become larger, as the resistance components of the interconnect increase.

Since some of poles keep away from the origin do not play important roles for the transient response, it is expected that for either short-length or high-resistive interconnects the number of dominant poles will become small, i.e., ef-

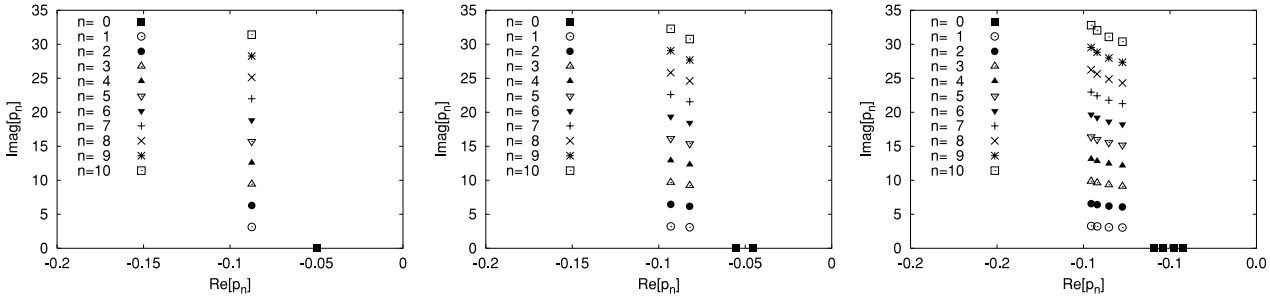

(a) $N = 1$ (b) $N = 2$ (c) $N = 4$

Fig. 7 Distribution of poles for N-conductor interconnects. The poles with negative imaginary part are not shown in this figure. ($r = 0.5\,[\Omega/\mathrm{mm}],\ d = 5.0\,[\mathrm{mm}]$)

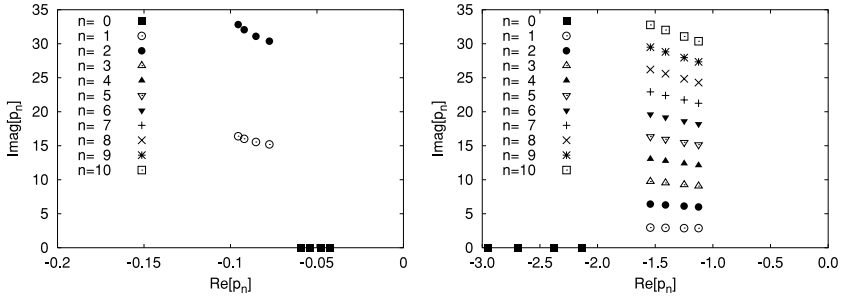

(a) $r = 0.5\,[\Omega/\mathrm{mm}],\ d = \mathbf{1.0}\,[\mathrm{mm}]$ (b) $r = \mathbf{25.0}\,[\Omega/\mathrm{mm}],\ d = 5.0\,[\mathrm{mm}]$

Fig. 8 Distribution of poles for 4-conductor interconnect for the cases that (a) the length d becomes short and (b) the resistance component r becomes large.

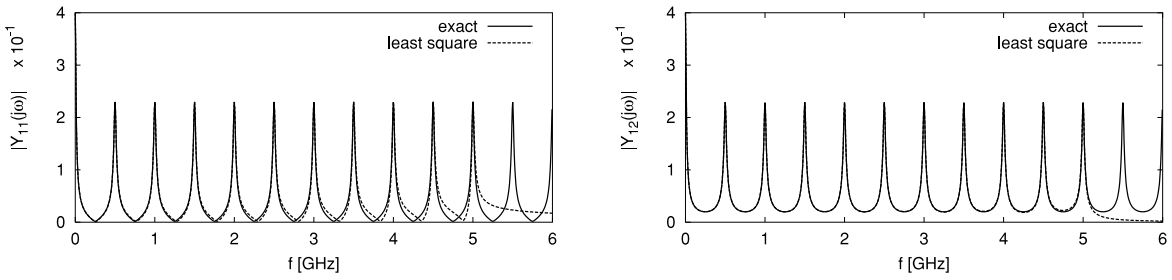

(a) $|Y_{11}(j\omega)|$ (b) $|Y_{12}(j\omega)|$

Fig. 9 Frequency response curves for single conductor interconnect. ($r = 0.5\,[\Omega/\mathrm{mm}]$, $d = 5.0\,[\mathrm{mm}]$, $f_{max} = 6.0\,[\mathrm{GHz}]$, $M = 10$)

fective reduction may be possible.

3.2 Calculation of Residues by Least Squares Method

We mention here the reason why the residues calculation procedure described in subsection 2.4 is required, through the following numerical results. Throughout our simulations, we set the real part of the complex frequency s_k as zero (i.e., $s_k = j\omega_k = j2\pi f_k$) in (24) and (25), and the sampling interval is taken to be 0.01 [GHz] equally.

Case 1: Let the highest frequency and the number of poles be $f_{max} = 6$ [GHz] and $M = 10$, respectively. In this case the frequency corresponding to the pole p_{10} (the suffix $i = 1$ is omitted) with largest imaginary part is about 5 [GHz]. The frequency response curve obtained by substituting the calculated poles and residues to the partial fraction (16) or (17) and the exact curve obtained from (7) are shown in Fig. 9. Here, the above-mentioned procedure of residues calculation is not used, and $|\hat{Y}_{12}(j\omega)|$ is calculated using the relation (18). The approximated curves by the partial fractions have relatively good agreement with the exact one up to 11-th peak around 5 [GHz], because we took a real pole and 10 of complex conjugate poles (i.e., $M = 10$). From the figure, it seems that the least squares fitting is successfully performed. However the calculated residues contain negative values as listed in the left-half of Table 1, which yields negative circuit parameters in (21). Thus, it is clear that the passivity is not satisfied in this case.

Case 2: For the case that the resistance component of interconnect becomes large, the least squares fitting fails to approximate the frequency-domain response accurately, as shown in Fig. 10. In this example, $|\hat{Y}_{12}(j\omega)|$ is also calculated using the relation (18). From these two examples, we can conclude that the pole selection in this manner is not suitable for our purpose.

Case 3: Next we tried to choose some extra poles beyond the highest frequency f_{max}. After choosing 6 of extra poles beyond $f_{max} = 6$ [GHz] (i.e., $M = 18$), the residues are calculated by performing the least squares fitting, which are listed in the right-half of Table 1 and the frequency response curves are shown in Fig. 11. As expected, $|\hat{Y}_{11}(j\omega)|$ matches the exact one within the whole frequency range ($0 \le f \le f_{max}$) of interest, as shown in Fig. 11(a). Unfortunately, as shown in Fig. 11(b), $|\hat{Y}_{12}(j\omega)|$ obtained from (17) and (18) is entirely different from the exact one. Furthermore, the values of $|\hat{Y}_{11}(j\omega)|$ at certain frequency range beyond the highest matched frequency ($f_{max} = 6$ [GHz]) become very large and differ completely from the exact one, as shown in Fig. 11(c). Note that the only difference of Figs. 11(a) and (c) is the scales of axes.

Table 1 Residues obtained by the least squares method for Cases 1 and 3.

	Case 1		Case 3	
n	$b_{1,n}$	$b_{0,n}$	$b_{1,n}$	$b_{0,n}$
1	3.815e−02	3.979e−03	4.000e−02	5.002e−03
2	3.815e−02	1.939e−03	4.000e−02	5.008e−03
3	3.816e−02	−1.568e−03	4.000e−02	5.017e−03
4	3.818e−02	−6.727e−03	4.000e−02	5.016e−03
5	3.820e−02	−1.385e−02	4.000e−02	5.004e−03
6	3.822e−02	−2.349e−02	4.000e−02	4.979e−03
7	3.825e−02	−3.664e−02	4.000e−02	4.940e−03
8	3.828e−02	−5.537e−02	4.000e−02	4.960e−03
9	3.829e−02	−8.508e−02	4.000e−02	5.049e−03
10	3.818e−02	−1.483e−01	4.000e−02	5.127e−03
11			4.000e−02	4.623e−03
12			3.990e−02	1.383e−02
13			4.149e−02	3.551e+00
14			1.704e+00	−1.005e+02
15			−1.902e+01	6.750e+02
16			6.859e+01	−1.764e+03
17			−9.761e+01	1.972e+03
18			4.815e+01	−7.910e+02

From the right-half of Table 1, the residues for $n > 12$, which correspond to the extra poles, contain negative or large values and consequently do not guarantee the passivity. Thus, it is concluded that disagreement of $|\hat{Y}_{12}(j\omega)|$ and huge values of $|\hat{Y}_{11}(j\omega)|$ at frequency range beyond f_{max} are due to the extra pole-residue pairs.

Case 4: In this example, to remove the pole-residue pairs beyond the highest frequency is considered. In the same conditions as Case 3, 6 extra pole-residue pairs for $n > 12$ are truncated and the frequency response curves are computed. The results are illustrated in Fig. 12. The effect of truncation begins to appear at the last half of the frequency range; that is, the accuracy of partial fractions (16) and (17) at higher frequency range is degraded. However, at lower

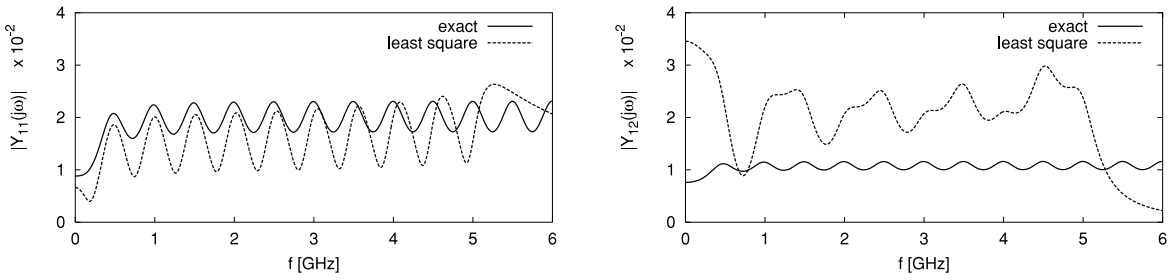

(a) $|Y_{11}(j\omega)|$ (b) $|Y_{12}(j\omega)|$

Fig. 10 Frequency response curves for single conductor interconnect. (r = **25.0** [Ω/mm], d = 5.0 [mm], f_{max} = 6.0 [GHz], M = 10)

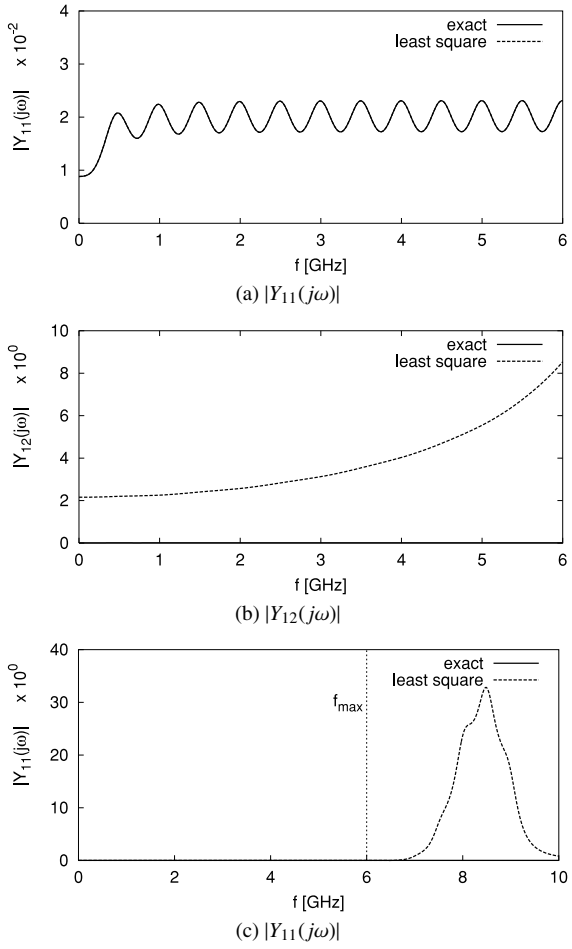

(a) $|Y_{11}(j\omega)|$ (b) $|Y_{12}(j\omega)|$ (c) $|Y_{11}(j\omega)|$

Fig. 11 Frequency response curves for the case that extra poles beyond f_{max} are used. (r = **25.0** [Ω/mm], d = 5.0 [mm], f_{max} = 6.0 [GHz], M = 18)

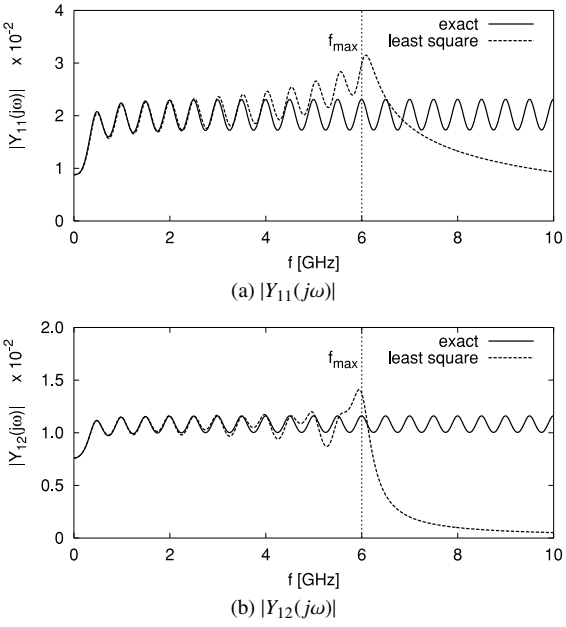

(a) $|Y_{11}(j\omega)|$ (b) $|Y_{12}(j\omega)|$

Fig. 12 Frequency response curves for the case that 6 poles beyond f_{max} are truncated. (r = **25.0** [Ω/mm], d = 5.0 [mm], f_{max} = 6.0 [GHz], M = 12, α = 6)

frequency range both curves remain matched. Furthermore the calculated response $|\hat{Y}_{12}(j\omega)|$ using the relation (18) is also matched to the exact one at lower frequency range, unlike the Case 3. Note that the partial fractions (16) and (17) (or the resulting asymptotic equivalent circuits) become more precise as the value of f_{max} increases, because matched frequency range becomes wide accordingly. Further it has been confirmed that positive residues and/or circuit elements of the macromodels can be obtained by increasing the number of extra poles, even if negative residues and/or circuit elements appeared around f_{max}.

In order to investigate the effect of the truncation and how to determine the number of extra poles α, we examined root mean square (rms) error between the exact and the approximated frequency responses in $0 \le f \le f_{max}$, with different line parameters, highest matched frequency f_{max} and number of extra poles α. The results are shown in Table 2, where the most right column indicates whether all passive elements have positive values or not when the extra pole-residue pairs are truncated. Note that the rms error of Y_{11} increases due to truncating the extra poles, while the one for Y_{12} always decreases. This coincides with the results shown in Figs. 11 and 12. When the same line parameters and different α are taken, the differences between the rms errors are small. Therefore, a small α is preferable from computational efficiency point of view. However, this does not necessarily obtain the passive macromodels as shown in Table 2. Roughly speaking, α depends on the number

Table 2 Root mean square error between the approximated and exact responses, where "truncated" and "not truncated" mean that the terms corresponding to the extra poles are truncated or not, and "True" and "False" in the column of passivity indicate that the obtained circuit is passive or not, respectively.

line parameters	f_{max} [GHz] (M)	α	rms error for Y_{11}		rms error for Y_{12}		Passivity
			not truncated	truncated	not truncated	truncated	
R = 25.0 [Ω/mm], L = 100.0 [nH/mm], C = 0.4 [pF/mm], G = 0.5 [mS/mm], d = 5.0 [mm]	5.0 (10)	3	2.911e−06	9.570e−04	1.053e−02	1.090e−04	False
		5	5.968e−08	9.552e−04	7.438e−02	1.061e−04	True
		10	4.420e−11	9.560e−04	3.847e+02	1.052e−04	True
		20	3.305e−11	9.560e−04	1.177e+05	1.051e−04	True
	10.0 (20)	3	9.816e−06	1.025e−03	1.945e−02	1.135e−04	False
		5	4.938e−07	1.021e−03	2.205e−01	8.557e−05	False
		10	8.583e−11	1.025e−03	7.327e+01	7.906e−05	True
		20	1.129e−10	1.025e−03	2.945e+05	7.907e−05	True
	15.0 (30)	3	1.767e−05	1.052e−03	2.623e−02	1.435e−04	False
		5	1.397e−06	1.044e−03	3.887e−01	8.303e−05	False
		10	8.882e−10	1.056e−03	2.090e+02	6.601e−05	True
		20	5.192e−11	1.055e−03	2.298e+05	6.607e−05	True
R = 0.5 [Ω/mm], L = 1.0 [nH/mm], C = 40.0 [pF/mm], G = 0.5 [mS/mm], d = 5.0 [mm]	5.0 (10)	3	3.699e−04	9.635e−02	8.652e−01	9.866e−03	False
		5	4.611e−06	9.575e−02	6.237e+00	1.066e−02	True
		10	1.568e−08	9.574e−02	1.023e+05	1.068e−02	True
		20	6.777e−08	9.574e−02	1.850e+08	1.068e−02	True
	10.0 (20)	3	1.591e−03	1.042e−01	1.565e+00	6.394e−03	False
		5	7.420e−05	1.028e−01	1.810e+01	7.926e−03	True
		10	6.906e−08	1.027e−01	8.539e+03	8.040e−03	True
		20	6.899e−08	1.027e−01	3.270e+08	8.040e−03	True
	15.0 (30)	3	3.031e−03	1.079e−01	2.085e+00	4.963e−03	False
		5	2.410e−04	1.059e−01	3.150e+01	6.459e−03	False
		10	1.301e−07	1.057e−01	1.821e+04	6.719e−03	True
		20	5.662e−08	1.057e−01	1.566e+08	6.719e−03	True
R = 25.0 [Ω/mm], L = 10.0 [nH/mm], C = 4.0 [pF/mm], G = 0.5 [mS/mm], d = 1.0 [mm]	5.0 (2)	3	3.271e−07	6.790e−03	1.513e−02	1.618e−03	True
		5	7.379e−10	6.789e−03	4.215e−02	1.619e−03	True
		10	1.965e−10	6.789e−03	1.083e+06	1.619e−03	True
		20	7.529e+05	6.789e−03	1.596e+06	1.619e−03	True
	10.0 (4)	3	3.736e−06	8.188e−03	3.310e−02	1.419e−03	True
		5	1.032e−08	8.180e−03	1.368e−01	1.429e−03	True
		10	4.771e−10	8.180e−03	5.440e+05	1.429e−03	True
		20	9.821e−10	8.180e−03	9.321e+05	1.429e−03	True
	15.0 (6)	3	1.283e−05	8.874e−03	5.124e−02	1.245e−03	True
		5	8.669e−08	8.854e−03	2.655e−01	1.270e−03	True
		10	6.770e−10	8.854e−03	2.420e+04	1.270e−03	True
		20	1.590e−10	8.854e−03	4.734e+06	1.270e−03	True
R = 25.0 [Ω/mm], L = 1.0 [nH/mm], C = 40.0 [pF/mm], G = 0.5 [mS/mm], d = 1.0 [mm]	5.0 (2)	3	1.911e−06	6.813e−02	9.103e−01	1.220e−02	False
		5	1.072e−09	6.473e−02	3.702e+00	1.424e−02	True
		10	1.005e−13	6.470e−02	9.716e+02	1.424e−02	True
		20	2.510e+02	6.470e−02	1.898e+02	1.424e−02	True
	10.0 (4)	3	1.493e−05	7.983e−02	1.519e+00	1.249e−02	False
		5	4.768e−08	7.866e−02	7.608e+00	1.211e−02	True
		10	6.061e−12	7.843e−02	1.021e+05	1.230e−02	True
		20	3.881e−12	7.843e−02	6.500e+04	1.230e−02	True
	15.0 (6)	3	4.096e−05	8.544e−02	2.115e+00	1.821e−02	False
		5	3.089e−07	8.611e−02	1.279e+01	1.012e−02	False
		10	5.741e−12	8.539e−02	1.006e+04	1.086e−02	True
		20	5.656e−12	8.539e−02	5.911e+04	1.086e−02	True

of poles which have the imaginary part less than or equal to $2\pi f_{max}$. With increase of the number of poles, M and α should be taken largely in order to obtain the passive macromodels. However, α is also dependent on the line parameters. Therefore, it is difficult to determine a suitable value of α in advance, and the proposed procedure provided in Subsect. 2.4 is necessary.

3.3 Transient Simulations

Now, let us calculate the transient responses for a simple linear circuit with a single-conductor interconnect shown in Fig. 13. The SPICE simulations using the asymptotic equivalent circuit of Fig. 4(a) are carried out with varying the highest matched frequency f_{max} (accordingly M is changed), and compared with the simulated results of built-in SPICE model. Figure 15 shows the transient response waveforms for $r = 0.5\,[\Omega/\mathrm{mm}]$ and $d = 5.0\,[\mathrm{mm}]$. All the waveforms have relatively good agreement, although ringing occurs at rising and falling edges of waveforms. The ringing can be suppressed with increasing M, but remarkable

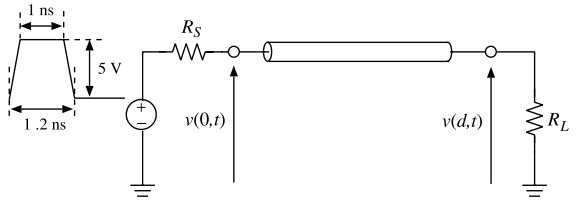

Fig. 13 Simple linear circuit with single conductor interconnect. (R_S = 10[Ω], R_L = 10[Ω])

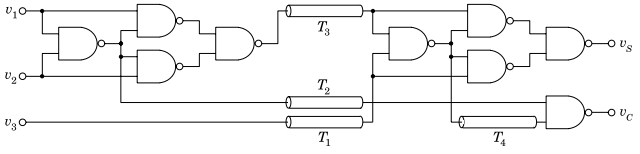

Fig. 14 Full-adder circuit. The parameters of all interconnects $T_1 \sim T_4$ are R = 500 [Ω/mm], L = 10 [μH/mm], C = 0.01 [pF/mm], G = 0.5 [μS/mm], d = 5 [mm].

changes are not observed even for M = 100 (in this case f_{max} = 50 [GHz]).

Figure 16 is the transient waveforms for the case that the resistance component r of interconnect was increased. In this case, the poles are far from the imaginary axis (see Fig. 8 (b)), but this does not affect the transient waveforms; that is, the number of poles M can not be reduced for the case of interconnect with high resistance component.

Next, after setting the length d of interconnect to be short, the transient simulation is carried out. In this case, the poles go far away from the real axis with n of (8), which is illustrated in Fig. 8(a). The transient waveforms for M = 10 (in this case f_{max} = 25 [GHz]) are approximately coincide with the SPICE results, as shown in Fig. 17. Thus, for the case of short-length interconnect, effective reduction is possible.

Finally, as an example of circuit with nonlinear element, a full-adder circuit shown in Fig. 14 is simulated and

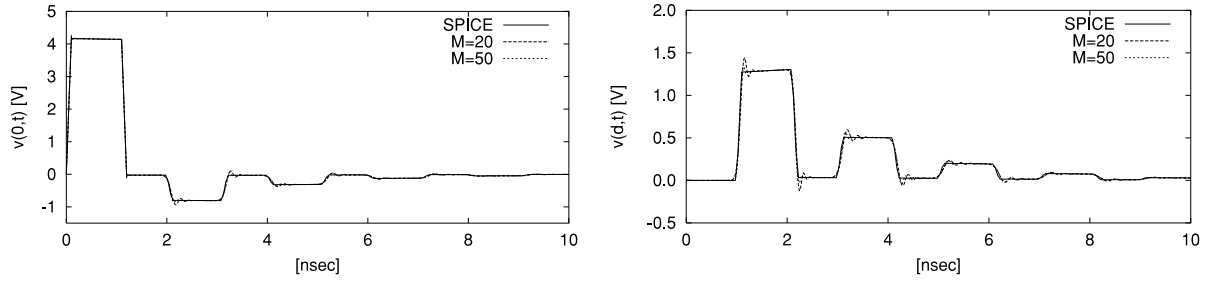

(a) Near end (b) Far end

Fig. 15 Transient response of the circuit shown in Fig. 13. (r = 0.5 [Ω/mm], d = 5.0 [mm])

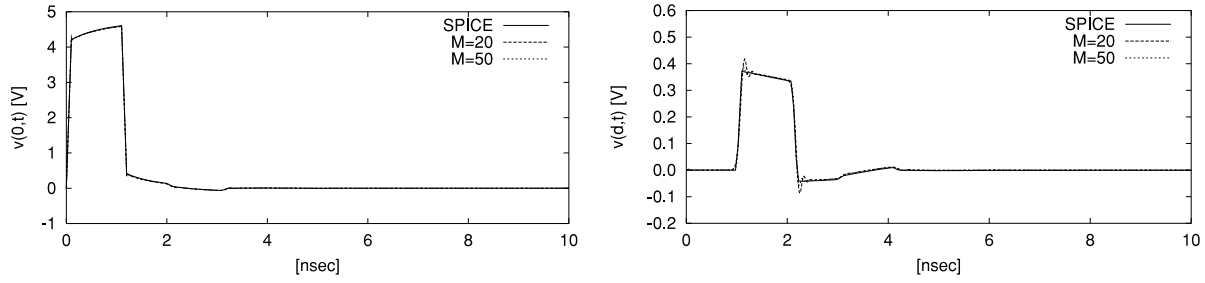

(a) Near end (b) Far end

Fig. 16 Transient response of the circuit shown in Fig. 13. (r = 25.0 [Ω/mm], d = 5.0 [mm])

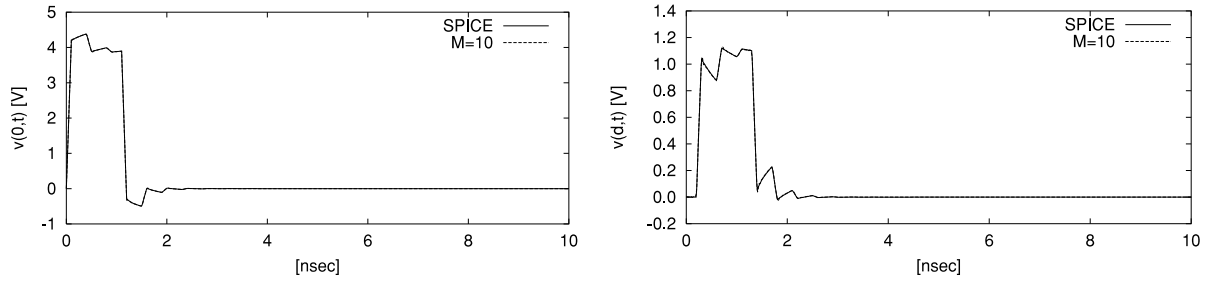

(a) Near end (b) Far end

Fig. 17 Transient response of the circuit shown in Fig. 13. (r = 25.0 [Ω/mm], d = 1.0 [mm])

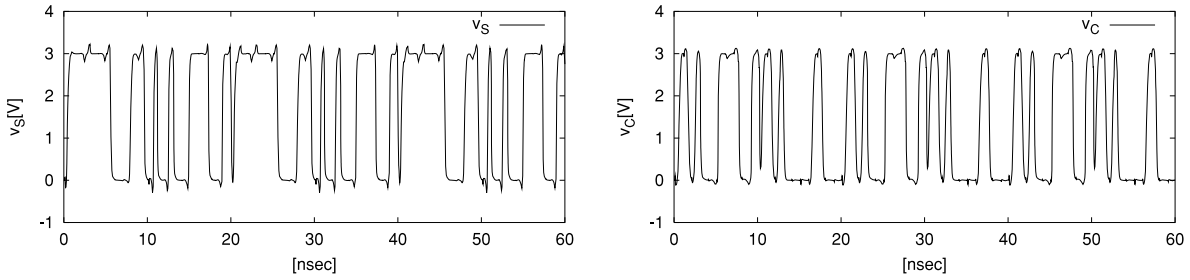

(a) v_S (b) v_C

Fig. 18 Transient response for the full-adder circuit shown in Fig. 14.

the results are illustrated in Fig. 18. Replacing the interconnect with the corresponding asymptotic equivalent circuit, where $M = 20$, effective simulation using SPICE is possible for nonlinear cases.

4. Conclusion

In this paper, we have proposed an algorithm for calculating the exact poles, the corresponding residues are estimated by the least squares method. A procedure for calculation of the residues that guarantee the passivity has also provided. Using the poles and residues, each element of the admittance matrix of interconnects is approximated by the partial fraction. Though the frequency response curves calculated using the partial fractions becomes inaccurate around the highest matched frequency f_{max}, the partial fractions and the resulting asymptotic equivalent circuit models are always passive. Further, it has been shown, from the investigations of pole distributions and the transient simulations, that the effective model-order reduction is possible for the case of short-length interconnects. Thus our method is efficiently applied for VLSIs.

References

[1] J.A. Brandao Faria, Multiconductor Transmission-Line Structures: Modal Analysis Techniques, John Wiley & Sons, 1993.
[2] M. Celik, L. Pileggi, and A. Odabasioglu, IC Interconnect Analysis, Kluwer Academic Pub., 2002.
[3] J.L. Wyatt, Jr., "Signal propagation delay in RC models for interconnect," Circuit Analysis, Simulation and Design, ed. A.E. Ruehli, pp.254–291, Elsevier Science Pub. B.V., North-Holland, 1987.
[4] W.C. Elmore, "The transient response of damped linear networks with particular regard to wideband amplifiers," J. Appl. Phys., vol.19, pp.55–63, Jan. 1948.
[5] T. Sakurai, "Closed-form expressions for interconnection delay, coupling, and crosstalk in VLSI's," IEEE Trans. Electron Devices, vol.40, no.1, pp.118–124, 1993.
[6] S.-Y. Kim, N. Gopal, and L.T. Pillage, "Time-domain macromodels for VLSI interconnect analysis," IEEE Trans. Comput.-Aided Des. Integr. Circuits Syst., vol.13, no.10, pp.1257–1270, 1994.
[7] R. Gupta, B. Tutuianu, and L.T. Pileggi, "The Elmore delay as a bound for RC trees with generalized input signals," IEEE Trans. Comput.-Aided Des. Integr. Circuits Syst., vol.16, no.1, pp.95–104, 1997.
[8] C.J. Alpert, A. Devgan, and C.V. Kashap, "RC delay metrics for performance optimization," IEEE Trans. Comput.-Aided Des. Integr. Circuits Syst., vol.20, no.5, pp.571–582, 2001.
[9] T. Kimura and M. Okumura, "An efficient reduction method of a substrate RC network model," IEICE Trans. Fundamentals, vol.E84-A, no.3, pp.698–704, March 2001.
[10] E. Chiprout and M.S. Nakhla, Asymptotic Waveform Evaluation and Moment Matching for Interconnect Analysis, Kluwer Academic Pub., 1994.
[11] E. Chiprout and M.S. Nakhla, "Analysis of interconnect networks using complex frequency hopping (CFH)," IEEE Trans. Comput.-Aided Des. Integr. Circuits Syst., vol.14, no.2, pp.186–200, 1995.
[12] Q. Yu, J. Meiling, and E.S. Kuh, "Passive multipoint moment matching model order reduction algorithm on multiport distributed interconnect networks," IEEE Trans. Circuits Syst. I, vol.46, no.1, pp.140–160, 1999.
[13] P. Feldmann and R.W. Freund, "Efficient linear analysis by Padé approximation via the Lanczos process," IEEE Trans. Comput.-Aided Des. Integr. Circuits Syst., vol.14, no.5, pp.639–649, 1995.
[14] A. Odabasioglu, M. Celik, and L.T. Pileggi, "PRIMA: Passive reduced-order interconnect macromodeling algorithm," IEEE Trans. Comput.-Aided Des. Integr. Circuits Syst., vol.17, no.8, pp.645–654, 1998.
[15] A. Ushida, K. Urabe, Y. Yamagami, and Y. Nishio, "Asymptotic equivalent circuits of interconnects based on complex frequency method," Proc. ECCTD'01, vol.3, pp.29–32, 2001.
[16] D.K. Faddeeva and V.N. Faddeeva, Computational Methods of Linear Algebra, W.H. Freeman and Co., 1963.
[17] J. Kawata, Y. Tanji, Y. Nishio, and A. Ushida, "Asymptotic equivalent circuits of interconnects and the passivity," IEICE Technical Report, NLP2003-134, 2003.
[18] Y. Yamagami, Y. Tanji, A. Hattori, Y. Nishio, and A. Ushida, "A reduction technique of large scale RCG interconnects in the complex frequency domain," Int. J. Circuit Theory Appl., (to appear).
[19] A. Yonemoto, T. Hisakado, and K. Okumura, "An improvement of convergence of FFT-based numerical inversion of Laplace transforms," Proc. ISCAS'02, vol.V, pp.769–772, 2002.
[20] W.T. Beyene and J.E. Schutt-Aine, "Efficient transient simulation of high-speed interconnects characterized by sampled data," IEEE Trans. Compon. Packag. Manuf. Technol. B, vol.21, no.1, pp.105–114, Feb. 1998.
[21] M. Celik and A.C. Cangellaris, "Efficient transient simulation of lossy packaging interconnects using moment-matching techniques," IEEE Trans. Compon. Packag. Manuf. Technol. B, vol.19, no.1, pp.64–73, Feb. 1996.
[22] K.L. Choi, N. Na, and M. Swaminathan, "Characterization of embedded passives using macromodels in LTTC technology," IEEE Trans. Compon. Packag. Manuf. Technol. B, vol.21, no.3, pp.258–268, Aug. 1998.
[23] T. Watanabe and H. Asai, "Synthesis of time-domain models for interconnects having 3-D structure based on FDTD method," IEEE Trans. Circuits Syst. II, vol.47, no.4, pp.302–305, April 2000.
[24] Y. Tanji and M. Tanaka, "Hierarchical least-squares algorithm for macromodeling high-speed interconnects characterized by sampled data," IEICE Trans. Fundamentals, vol.E83-A, no.9, pp.1833–1843,

Sept. 2000.
[25] M. Suzuki, H. Miyashita, A. Kamo, T. Watanabe, and H. Asai, "A synthesis of time-domain interconnect models by MIMO type of selective orthogonal least-square method," IEEE Trans. Microw. Theory Tech., vol.49, no.10, pp.1708–1714, Oct. 2001.

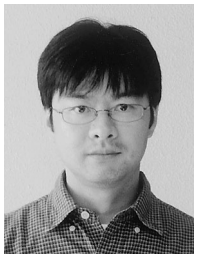

Junji Kawata received the B.E., M.E., and Ph.D. degrees from Tokushima University, Tokushima, Japan, in 1990, 1992 and 2001, respectively. Since 1992, he has been with the Department of Mechanical and Electronic Engineering at Tokushima Bunri University, where he is currently a Lecturer. His research interests are in circuit simulation and chaotic communication. Dr. Kawata is a member of the IEEE.

Yuichi Tanji received the B.E., M.E., and Ph.D. degrees from Tokushima University, Tokushima, Japan, in 1993, 1995 and 1998, respectively. After graduation, he held Research Associate positions at Sophia University and Kagawa University, and is currently an Associate Professor of the Department of Reliability-based Information Systems Engineering at Kagawa University. His research interests are in circuit simulation, artificial neural networks, and image and signal processing. Dr. Tanji is a member of the IEEE.

Yoshifumi Nishio received the B.E., M.E., and Ph.D. degrees in electrical engineering from Keio University, Yokohama Japan, in 1988, 1990, and 1993, respectively. In 1993, he joined the Department of Electrical and Electronic Engineering at Tokushima University, Tokushima Japan, where he is currently an Associate Professor. From May 2000 he spent a year in the Laboratory of Nonlinear Systems (LANOS) at the Swiss Federal Institute of Technology Lausanne (EPFL) as a Visiting Professor. His research interests include analysis and application of chaos in electrical circuits, analysis of synchronization in coupled oscillators circuits, development of analyzing methods for nonlinear circuits and theory and application of cellular neural networks. He is currently the Chair of the IEEE CAS Technical Committee on Nonlinear Circuits and Systems (NCAS) and the Secretary of the IEICE Research Society of Nonlinear Theory and its Applications (NOLTA). He is serving as an Associate Editor for the IEEE Transactions on Circuits and Systems - Part I, for the area of Theory and Systems. He is a member of the IEEE and the RISP.

Akio Ushida received the B.E. and M.E. degrees in electrical engineering from Tokushima University in 1961 and 1966, respectively, and the Ph.D. degree in electrical engineering from University of Osaka Prefecture in 1974. He was an associate professor from 1973 to 1980 at Tokushima University. From 1980 to 2003, he was a Professor in the Department of Electrical Engineering at Tokushima University. Since 2003, he has been with the Department of Mechanical and Electronic Engineering, Tokushima Bunri University. From 1974 to 1975 he spent one year as a visiting scholar at the Department of Electrical Engineering and Computer Sciences at the University of California, Berkeley. His current research interests include numerical methods and computer-aided analysis of nonlinear system. Dr. Ushida is a member of the IEEE.